2015

Understanding phase transformations in steels using modern electron microscopy techniques

Elena V. Pereloma
University of Wollongong, elenap@uow.edu.au

Ahmed A. Saleh
University of Wollongong, asaleh@uow.edu.au

Hendrik T. Spanke
University of Wollongong

Fayez Al-Harbi
University of Wollongong, fa854@uowmail.edu.au

Azdiar A. Gazder
University of Wollongong, azdiar@uow.edu.au

Publication Details

Pereloma, E. V., Saleh, A. A., Spanke, H. Th., Al-Harbi, F. & Gazder, A. A. (2015). Understanding phase transformations in steels using modern electron microscopy techniques. Asia Steel International Conference (Asia Steel 2015): proceedings (pp. 68-71). Japan: Iron and Steel Institute of Japan.

Understanding phase transformations in steels using modern electron microscopy techniques

Abstract
The advantages and limitations of electron back-scattering diffraction coupled with energy dispersive X-ray spectroscopy and of transmission Kikuchi diffraction in relation to the in-depth characterisation of steel microstructures containing phases with similar lattice parameters and/or precipitates are discussed. An in-house developed EBSD map post-processing methodology provided insights into the mechanisms of bainite formation.

Disciplines
Engineering | Science and Technology Studies

Publication Details
Pereloma, E. V., Saleh, A. A., Spanke, H. Th., Al-Harbi, F. & Gazder, A. A. (2015). Understanding phase transformations in steels using modern electron microscopy techniques. Asia Steel International Conference (Asia Steel 2015): proceedings (pp. 68-71). Japan: Iron and Steel Institute of Japan.

Understanding phase transformations in steels using modern electron microscopy techniques

Elena V. Pereloma[1,2*], Ahmed A. Saleh[1], Hendrik Th. Spanke[1], Fayez Al-Harbi[1], Azdiar A. Gazder[2]

[1] School of Mechanical, Materials and Mechatronics Engineering, University of Wollongong, New South Wales 2522, Australia

[2] Electron Microscopy Centre, University of Wollongong, New South Wales 2500, Australia

Abstract: The advantages and limitations of electron back-scattering diffraction coupled with energy dispersive X-ray spectroscopy and of transmission Kikuchi diffraction in relation to the in-depth characterisation of steel microstructures containing phases with similar lattice parameters and/or precipitates are discussed. An in-house developed EBSD map post-processing methodology provided insights into the mechanisms of bainite formation.

1. INTRODUCTION

The microstructures of low alloyed steels commonly contain a mixture of different body centred cubic (bcc) and body centred tetragonal (bct) phases such as polygonal ferrite (PF), bainitic ferrite (BF), irregular-shaped ferrite in granular bainite (GB) and martensite. However the small changes in the *a* and *c* parameters of these bct lattices (caused by a variation in their carbon content) are imperceptible during the automated indexing of electron back-scattering patterns and result in them being routinely indexed as bcc iron during electron back-scattering diffraction (EBSD) mapping. This poses a significant problem during the quantification and detailed characterisation of the various phases present; as the microstructural constituents may look different upon visual inspection but they all belong to the bcc iron phase in the map. In some cases, this limitation of EBSD can be successfully overcome if simultaneous EBSD and energy dispersive X-ray spectroscopy (EDS) is undertaken [1, 2]. In other cases, specially developed post-processing methodologies segment the phases on the basis of their clearly distinct morphological characteristics or other EBSD-based identifiable differences such as band slope, band contrast, aspect ratio, internal misorientation, etc. (see Ref. [2] and the references therein).

While the spatial resolution of EBSD maps from bulk samples in conventional scanning mode is limited to ~30-50 nm due to the interaction volume effect, the 5-10 nm spatial resolution of the band contrast maps obtained via transmission Kikuchi diffraction (TKD) is comparable to conventional scanning transmission electron microscopy imaging [3, 4]. In this paper the simultaneous EBSD+EDS, TKD techniques and new post-processing methodologies have been applied to characterise low alloy strip, transformation-induced plasticity (TRIP) and quench and tempered (Q&T) steels. The advantages and limitations of each these novel techniques are discussed from a phase transformation mechanism point of view.

2. EXPERIMENTAL AND ANALYTICAL PROCEDURE

The compositions of the studied steels are shown in Table 1. Only the main alloying elements are listed for the strip and Q&T plate. The TRIP steel was subjected to thermo-mechanical processing using a Gleeble 3500 machine (for details see Refs. [2, 5]) whereas the strip and plate steels were received from BlueScope Steel Ltd. in as-processed condition.

Table 1. Chemical composition of the steels (wt.%).

	C	Mn	Si	Al	P
TRIP	0.15	2.00	0.30	1.00	0.05
Strip	0.162	0.75	0.007	0.035	0.01
Plate	0.16	1.2	0.45	0.03	0.021

* Corresponding author. E-mail: elenap@uow.edu.au, telephone: +61 2 4221 5507.

EBSD, EDS and TKD were conducted on a JEOL–JSM7001F field emission gun SEM equipped with a Nordlys-II(S) detector, an 80 mm^2 X-Max EDS detector and the Oxford Instruments AZtec acquisition software suite. Accelerating voltages and probe currents of 15 kV, 3.1 nA and 30 kV, 10 nA were used for EBSD, EBSD+EDS and TKD, respectively. A working distance of 12 mm was maintained constant irrespective of mapping technique. Step sizes of 95, 150 and 15 nm were used for the conventional scanning EBSD maps of TRIP, strip and plate steels, respectively. Alternatively, step sizes of 10 and 7.5 nm were used for the TKD maps of TRIP and plate steels, respectively. The EDS settings were a 20 keV energy range, auto-selecting the number of channels, a process time of 3 and a detector dead time of ~45-50%. Additionally, the TKD for the TRIP and plate steels was undertaken using thin foils at 40° stage and -50° specimen tilts. In all maps, RD = horizontal; ND = vertical.

The Oxford Instruments Channel-5^{TM}, MTex and Gatan DigitalMicrograph software packages were used for data analysis; as described in detail in Refs. [2,5]. Low-angle boundaries (LAGBs) are defined as misorientations between $2° \leq \theta < 15°$ whereas high-angle boundaries (HAGBs) extend from $\theta \geq 15°$ and $\Sigma 3$ twin boundaries are characterised by the 60°<111> axis-angle relationship. Subgrain/grain reconstruction was undertaken using 2° as the minimum misorientation in order to fix the angular resolution limit and retain orientation contrast information.

3. RESULTS AND DISCUSSION

3.1. Segmentation of bcc phases

The microstructure of the TRIP steel is a complex mixture of PF, carbide-free bainites, retained austenite (fcc, RA) and martensite. Although a challenging task, the in-house developed multi-step segmentation procedure (using a combination of (sub)grain orientation spread and size criteria [2,5]) was able to successfully segment the phases present in the microstructure (Fig. 1(a)). Whereas the segmentation of unlike phases such as PF and martensite was relatively easy to accomplish, differentiating phases with approximately similar morphological and orientation characteristics (such as the ferrites in GB and BF) was far more difficult as the band contrast and slope parameters are not sensitive enough to distinguish between alike structures via thresholding.

The EDS sensitivity to slight variations in carbon content when conducted simultaneously with EBSD mapping has led to further improvements in the phase segmentation technique by implementing a specially developed procedure in DigitalMicrograph [2]. Fig. 1(c) shows the differences in high and low carbon content in strip steel coiled at 560 °C and clearly indicates the location of these carbon-rich areas at either along grain boundaries or within small grains. It is speculated that the small grains with high carbon content may be martensite islands in GB whereas the carbon segregated at bainitic interfaces is in accordance with carbon diffusion out of supersaturated solid solution [6].

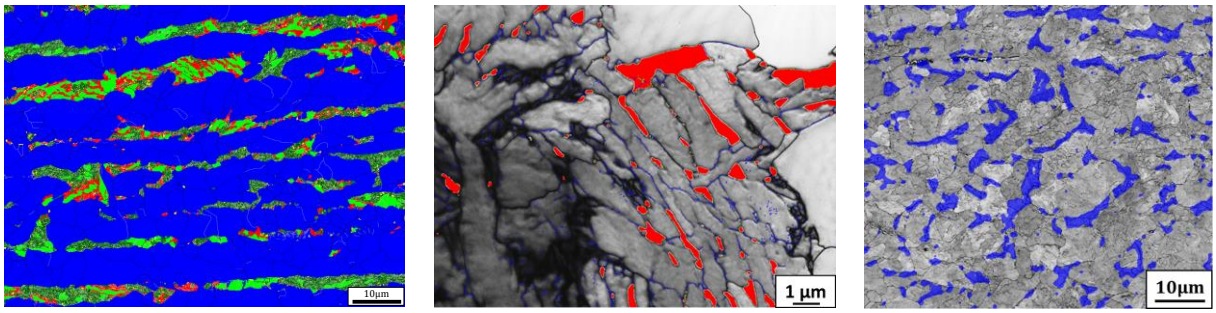

a b c

Fig. 1 (a) Segmented phases in TRIP steel (red = fcc, blue = PF, dark green = ferrite in GB, light green = BF laths and yellow = martensite), (b) TKD of TRIP steel (red = fcc, grey = bcc and black = unindexed (presumably martensite)) and (c) overlay of carbon-rich regions (blue) via EBSD+EDS on band contrast of strip steel. Black = HAGBs, silver = LAGBs.

As reported in Ref. [2], ferrite in GB has a higher carbon content compared to BF laths and both of them exhibit carbon enrichment compared to PF. Polygonal ferrite forms by diffusion-controlled phase transformation with a carbon content corresponding to the equilibrium phase diagram (~0.02 wt.%). On the other hand, bainite and martensite form by the displacive mechanism [6] and inherit a high

carbon content from austenite. It is now well documented via atom probe tomography that even after prolonged holding times following bainite formation, the bainitic ferrite matrix (free of visible defects and clusters) in TRIP [7,8] and nanobainitic [9,10] steels remains supersaturated with carbon. Bhadeshia [11] recently suggested that this could be due to the tetragonal nature of the BF lattice; which in turn has a higher solubility for carbon than the bcc one. On the other hand, the variation in carbon concentration in the ferrites in GB and BF is explained [2] by the formation of GB at a higher temperature than BF and by the differences in the diffusion path for carbon in GB and BF due to the distribution of RA grains (i.e. – the longer distance to the sparse RA in GB compared to the much shorter distance to the interlayers of RA in BF). As a result, carbon forms Cottrell atmospheres at dislocations in GB while it preferentially diffuses into the adjacent RA interlayers in BF.

The ability to correctly and reproducibly segment bainite morphologies in TRIP steel also provides the necessary basis for the detailed analysis of the crystallography of ferrite in GB and BF. As shown in [5], there is a distinct difference in the variant selection between these two morphologies such that a more limited number of crystallographic packets and variants is characteristic of BF but not of GB. Fig. 2 highlights the above mentioned differences in the crystallography of the ferrites in GB and BF formed in the same prior austenite grain. As shown in Fig. 2(f), the BF is characterised by the realisation of one or two crystallographic variants of BF laths within a particular packet (for example, CP2 and CP4-1 comprise variants 11 and 20, respectively (Fig. 2(b)). On the other hand, all six variants were realised in CP1 in GB (Figs. 2(b) and 2(e)). Although Fig. 2(f) could imply that a larger number of variants are present in some BF packets, it is pointed out that while some of these variants belong to the same packet type, they are located in spatially separated areas of the microstructure (see CP4-1 and CP4-2 in Fig. 2(b)). On some occasions, the variants also appear protrude from underneath the surface. Thus, for a complete analysis of bainite crystallography, 3D investigations are required.

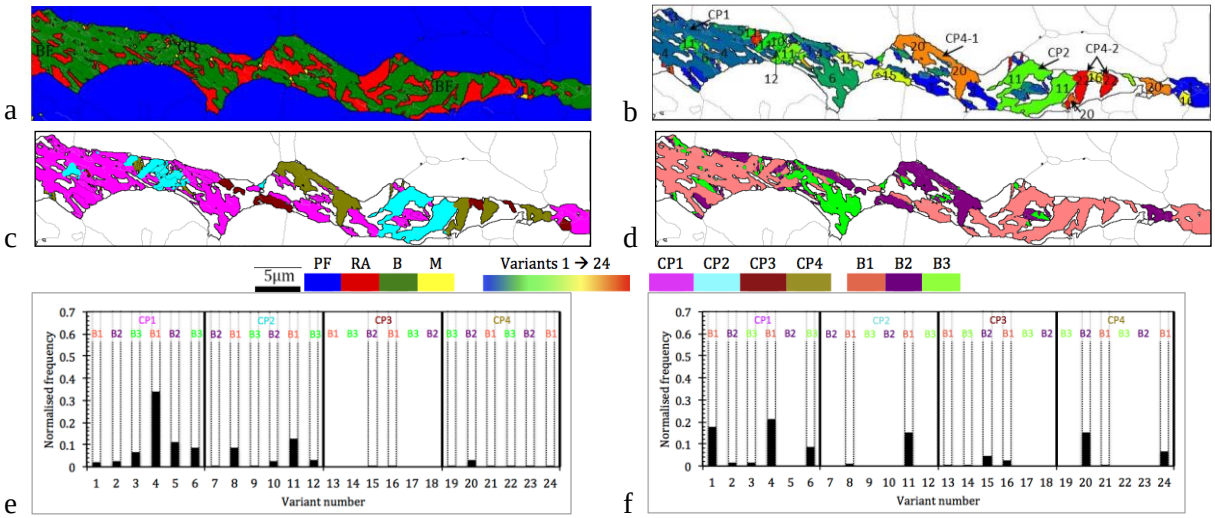

Figure 2: Crystallography of BF laths and GB in TRIP steel shown via (a) phase, (b) variants, (c) crystallographic packets (CP1-CP4) and (d) Bain groups (B1-B3). Normalised frequencies of the variants for (e) GB and (f) BF. In (a-d) thick black lines = interphase boundaries; (e, f) dashed lines = realised variants.

The dominance of nucleation events during continuous cooling and the self-accommodation of transformation strain are responsible for the realisation of the majority of variants in the ferrite of GB. On the other hand, the transformation strain is accommodated by the thick RA interlayers in BF; negating the need for self-accommodation and leading to strong variant selection.

3.2. Conventional scanning EBSD versus TKD

The TKD map for TRIP steel is shown in Fig. 1(b). Compared to the conventional EBSD map (Fig. 1 (a)), the TKD map area is smaller but due to electron transparent foil, the beam interaction volume is markedly reduced; thereby allowing for higher spatial resolution. Mapping via TKD using sizes as small as 7.5 nm provide reliable data on the features and constituents present in the microstructure such that much finer RA was identified at interfaces and between BF laths than in Fig. 1(a).

a 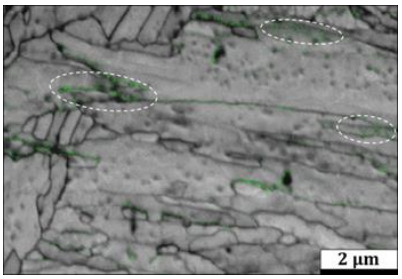

b 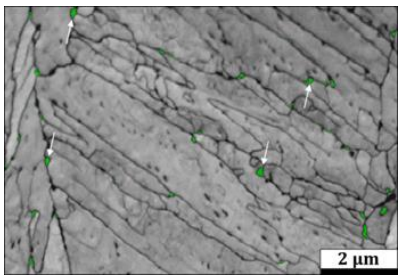

Fig. 3 High resolution (a) EBSD and (b) TKD band contrast maps of quenched and tempered steel with cementite overlaid in green.

Representative high resolution EBSD and TKD phase maps of Q&T steel are shown in Figs. 3(a) and 3(b), respectively. In Fig. 3(a), EBSD mapping on a thin foil was undertaken to minimise the interaction volume effect between the bainite/martensite (iron bcc) matrix and the cementite precipitates that formed during tempering. However, this EBSD map still suffered from two major drawbacks: (i) the morphology of the precipitates is not well defined such that cementite is indexed as random pixels (see the white ovals in Fig. 3(a)), and (ii) the crystallographic analysis of the orientation relationship (OR) between the bcc matrix and the cementite precipitates deviated away from all well-known ORs. In this regard, the TKD technique had two advantages: (i) some cementite precipitates were indexed as distinct structures at the boundaries (see the white arrows in Fig. 3(b)), and (ii) the Isaichev OR [12] was successfully and consistently identified. On the other hand, TKD failed to index cementite within the laths. This can be ascribed to: (i) the variation in the location of cementite through the foil thickness and the diffraction information being limited to near the bottom surface of the foil, and (ii) the diffraction characteristics being markedly different in the lath interiors compared to the lath boundaries.

4. CONCLUSION

Continuous progress in the development of both acquisition and data processing EBSD/TKD/EDS methodologies has advanced our understanding of microstructure development and phase transformations in steels. The obtained experimental evidence highlighted the difference in crystallography and composition of ferrite in two carbide-free bainite morphologies. For the first time, cementite was identified as a contiguous structure using TKD. The precision of orientation information enabled the successful and consistent identification of the Isaichev orientation relationship between cementite and the ferrite matrix.

Acknowledgements: This work was financially supported by the BlueScope Steel Metallurgy Centre, ARC HUB for Australian Steel Manufacturing and Engineering Materials Research Strength at the University of Wollongong. The JEOL JSM-7001F FEG-SEM was funded by the Australian Research Council grant LE0882613.

REFERENCES

[1] S. Zaefferer, P. Romano: Microsc. Microanal., 13 (2007), 944–945.
[2] A.A. Gazder, F. Al-Harbi, H.Th. Spanke, D.R.G. Mitchell, E.V. Pereloma: *Ultramicrosc.*, 147 (2014), 114-132.
[3] R.R. Keller, R. H. Geiss: J. Microsc.**,** 245 **(**2012), 245-251.
[4] P. W. Trimby: *Ultramicrosc.*, 120 (2012), 16-24.
[5] E. Pereloma, F. Alharbi, A.A. Gazder: J. Alloy. Comp. 615 (2014), 96-110.
[6] H.K.D.H. Bhadeshia: Bainite in steels: transformations, microstructure and properties, 2nd ed., IOM Communications Ltd., London, UK (2001), 1-454.
[7] E. Pereloma, I.B. Timokhina, M.K. Miller, P.D. Hodgson: Acta Mater., 55 (2007), 2587-2598.
[8] E. Pereloma, H. Beladi, L.-C. Zhang, I. Timokhina: Metall. Mater. Trans., A43 (2012), 3958–3971.
[9] F.G. Caballero, M.K. Miller, C. Garcia-Mateo, J. Cornide, M.J. Santofimia: Scr. Mater., 67 (2012), 846–849.
[10] F.G. Caballero, M.K. Miller, C. Garcia-Mateo, J. Cornide: J. Alloys Compd. 577(Suppl.1) (2013), S626–S630.
[11] H.K.D.H. Bhadeshia: Philos. Mag., 93 (2013), 3714–3725.
[12] I.V. Isaichev: Zh. Tekhn. Fiz., 17 (1947), 835-838.